



ELSEVIER

Contents lists available at ScienceDirect

## Signal Processing

journal homepage: [www.elsevier.com/locate/sigpro](http://www.elsevier.com/locate/sigpro)

# Optimum crossing-point estimation of a sampled analog signal with a periodic carrier

Graeme Smecher, Benoît Champagne \*

Department of Electrical and Computer Engineering, McGill University, Canada

## ARTICLE INFO

### Article history:

Received 11 March 2010  
 Received in revised form  
 16 October 2010  
 Accepted 25 February 2011  
 Available online 8 March 2011

### Keywords:

MAP estimation  
 MMSE estimation  
 Event-triggered sampling  
 Level-crossing  
 Pulse-width modulation  
 Cramér–Rao bound

## ABSTRACT

The problem of estimating the crossing points of a continuous-time random process, represented by a sequence of uniformly spaced noisy samples, with a periodic analog carrier signal is of crucial importance in the implementation of pulse-width modulation (PWM) and other event-triggered sampling systems. In this paper, we formally approach this problem from a statistical signal processing perspective under a Bayesian framework. We derive the maximum a posteriori (MAP) estimator of the crossing point from a finite sequence of noisy observations, along with a close approximation based on minimum mean squared error (MMSE) considerations. We also study the Bayesian Cramér–Rao bound (CRB) on attainable mean square estimation error. Finally, simulations of a PWM scenario demonstrate that both the MAP and MMSE estimators approach the CRB and outperform several benchmark estimators. The MMSE is a particularly attractive solution as it offers a computationally efficient approximation to the MAP estimator.

© 2011 Elsevier B.V. All rights reserved.

## 1. Introduction

In many signal processing applications, noisy samples of a continuous-time signal are used to estimate the times at which this signal crosses a known continuous-time function. The known function is typically zero, a fixed (non-zero) level, or a periodic carrier waveform, such as a sinusoidal or sawtooth signal. Zero-crossings are of interest in pitch detection [1,2], spectral analysis [3–5], and signal demodulation [6–8]. Level-crossings have been extensively studied [9], and are of practical interest in non-uniform sampling applications [10,11]. Carrier-crossings have also received substantial theoretical treatment [12,13] and are of practical interest in event-triggered sampling, including pulse-position modulation [14] and pulse-width modulation (PWM) [15,16].

In PWM, as applied to e.g. digitally controlled switching amplifiers, the crossing points of a bandlimited signal with a periodic carrier must be accurately determined to produce a high-fidelity output [17]. The analysis of PWM signals derived from random inputs has been considered from different perspectives, including: frequency spectrum [18,19], aliasing effects [20,21] and harmonic distortion [22]. Within the PWM framework, discrete-time crossing-point estimation is typically cast as a 2-step interpolation problem, where: (1) crossing points are coarsely located and (2) nearby samples are interpolated to generate more accurate estimates. The most commonly adopted choice for the interpolator in the 2nd step is the unique polynomial of order  $M-1$  passing through  $M$  sample points of the random signal. Linear interpolation is simple to implement but result in higher level of sampling errors and distortion [23]. The use of higher-order interpolation is usually favored as it offers a more flexible trade-off between complexity and performance. This includes quadratic [24], cubic [15,25] as well as higher-order polynomial and band-limited interpolation [26–28].

\* Corresponding author.

E-mail addresses: [graeme.smecher@mail.mcgill.ca](mailto:graeme.smecher@mail.mcgill.ca) (G. Smecher), [benoit.champagne@mcgill.ca](mailto:benoit.champagne@mcgill.ca) (B. Champagne).

In the context of switching amplifiers, audio quality depends directly on the accuracy of the crossing-point estimation [16]. Under a maximum distortion constraint, any loss in accuracy must be compensated by an increase in the over-sampling ratio, which in turn entails additional implementation costs. While the above interpolation approaches are often motivated by computational considerations, it is unclear under which conditions they perform optimally. In addition, none of these methods take explicit advantage of the statistical knowledge usually available about the underlying signal and noise in applications. Therefore, while they may perform adequately in an over-sampled regime when the random signal is low-pass in nature, they do not generalize to arbitrary signal models, and may not be as effective as alternatives derived from well-established optimality criteria.

In this paper, we approach the discrete-time crossing-point estimation problem from a statistical signal processing perspective under a Bayesian framework [29]. We consider a general formulation applicable to a large class of systems (including traditional PWM), in which the observed signal samples are modeled as the sum of a Gaussian random process and an independent noise component. Making use of an Edgeworth's type of expansion [30], we derive conditions under which the distribution of the noisy signal samples can be adequately modeled by a Gaussian distribution. This includes two practical scenarios: low-power uniform quantization noise, and spectrally shaped quantization noise. Making use of the Gaussian approximation along with basic properties of the carrier waveform, we derive the maximum a posteriori (MAP) crossing-point estimator as well as a minimum mean squared error (MMSE) estimator. The latter is shown to be a computationally efficient approximation to the former under high SNR condition. We also investigate fundamental performance limits on the crossing-point estimator by deriving the Bayesian Cramér–Rao bound (CRB) on the lowest achievable mean square error (MSE). Finally, through simulation experiments of a general PWM scenario, we show that the MAP and MMSE estimators outperform several crossing-point estimators selected from the literature.

The remainder of this work is organized as follows. In Section 2, the crossing-point estimation problem and the associated signal model are defined. In Section 3, we derive both the MAP and MMSE estimators of the crossing point, while in Section 4, we investigate performance issues including the Bayesian CRB and computational cost. In Section 5, we present the results of Monte Carlo simulations focusing on a generalized PWM scenario. We conclude with Section 6. A proof is included in Appendix.

## 2. Problem formulation

Let  $s(t)$  be a continuous-time, real-valued, wide-sense stationary (WSS) Gaussian random process with zero mean, autocorrelation function  $r_s(t-u) = E\{s(t)s(u)\}$ , and variance  $\sigma_s^2 = r_s(0)$ . Let  $y(t)$  be a known, deterministic reference signal in the form of a periodic carrier. We wish to determine the crossing points of  $s(t)$  and  $y(t)$ , or equivalently, the zero-crossings of  $z(t) \triangleq s(t) - y(t)$ . In the discrete-time problem, only a sequence of uniformly

spaced noisy samples from  $s(t)$  is available, as given by

$$x[k] \triangleq s(kT_s) + n[k], \quad k \in \mathbb{Z}, \quad (1)$$

where  $T_s$  is the sampling period and  $n[k]$  is the quantization noise.

In high-precision applications with a large number of bits, it is a common practice to model individual quantization noise samples as uniformly distributed random variables [31]. In lower precision systems where a linear noise shaping stage is employed prior to crossing-point detection, the filtered quantization noise is commonly approximated by a Gaussian distribution. This is a consequence of the central limit theorem as applied to the output of the noise shaping filter and is well documented in the technical literature. In particular, the fact that non-Gaussian inputs tend to become nearly Gaussian as a result of linear filtering is discussed in general terms in [32,33], while the specific case of noise shaping in delta-sigma analog-to-digital converter structures is considered in [34–36].

Adjacent noise samples may also exhibit a certain degree of correlation: for example, in PWM for audio amplifier applications, the signal samples are created by upsampling of a digital audio signal with original sampling rate of 44.1 kHz [16]. In this work, we model the noise sequence  $n[k]$  as a WSS discrete-time random process with zero mean, autocorrelation function  $r_n[k-1]$  and variance  $\sigma_n^2 = r_n[0]$ . To accommodate various situations of interest, we make *no specific assumption* about the statistical distribution of the noise samples  $n[k]$ ; however, we assume that the system operates at moderate to high SNR, i.e.  $\sigma_s^2 > \sigma_n^2$ , a condition satisfied in most applications. Finally, we assume that the signal and noise components are independent.

Given the periodic carrier  $y(t)$  and the sequence of noisy samples  $x[k]$  (for  $k \geq 0$ ), we seek to estimate the sequence of points  $0 < \tau_0 < \tau_1 < \dots$  satisfying  $s(\tau_i) = y(\tau_i)$ . Because the observation time and thus the number of crossing points are unlimited, the complexity of the estimation problem is unbounded. To bring the problem into a simpler form, we follow a standard approach [23,28], and impose a two-step structure on the solution as shown in Fig. 1: first, we coarsely locate crossing points using estimator  $E_1$ ; next, we apply a refined estimator  $E_2$  in the neighborhood of each crossing point to generate a more accurate estimate.

Estimator  $E_1$  can be realized by monitoring for sign changes of

$$d[k] = x[k] - y(kT_s) = z(kT_s) + n[k] \quad (2)$$

within each period of the carrier waveform  $y(t)$ . When the noise term is small and the samples are closely spaced, the times at which  $d[k]$  changes sign, as given by  $k_i$  satisfying  $d[k_i-1]d[k_i] < 0$ , coarsely bound each zero-crossing  $\tau_i$  to a single sample interval  $T_s$  as follows:

$$\tau_i \in \mathcal{T}_i \triangleq ((k_i-1)T_s, k_iT_s). \quad (3)$$

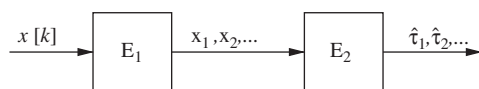


Fig. 1. Two-step approach to crossing-point estimation.

Because analog signal  $z(t)$  remains close to zero in the immediate vicinity of a zero-crossing and the quantization noise  $\eta[k]$  may change the sign of its sample values  $z(kT_s)$  in (2), this approach may result in erroneous decisions, including: missed zero-crossings and false estimation of the coarse interval  $\mathcal{T}_i$ . In practice, however, these conditions can be eluded by a proper system design. For instance, missed detection within a carrier period is completely avoided by selecting a carrier pulse shape that spans the whole dynamic range of signal amplitudes, while the number of erroneous  $\mathcal{T}_i$  can be kept below an acceptable level by increasing the SNR or the rate of change of  $y(t)$ .

We also note that traditional PWM systems using single-edge and double-edge modulation, where the carrier period, respectively, spans one and two sampling intervals, automatically guarantee a single crossing point per sample, so that the coarse estimator  $E_1$  is not necessary, i.e. it is implicitly built into  $y(t)$  [17]. Motivated by these considerations, we assume in our theoretical developments that  $E_1$  operates satisfactorily and focus on the refined estimator  $E_2$ . This approach is further motivated by the fact that  $E_2$  has the ability to correct small errors in the output of  $E_1$ .

We now restrict our attention to samples immediately surrounding  $\mathcal{T}_i$ . We form the  $M$ -dimensional vectors  $\mathbf{x}_i$  using  $M_1$  consecutive samples of  $x[k]$  preceding  $\tau_i$  and  $M_2 = M - M_1$  samples immediately following  $\tau_i$ :

$$\mathbf{x}_i = [x[k_i - M_1], \dots, x[k_i - 1], x[k_i], \dots, x[k_i + M_2 - 1]]^T, \quad (4)$$

where the superscript  $T$  denotes transposition. Estimator  $E_2$  must solve the following simplified problem: Given the carrier signal  $y(t)$ , the sample vector  $\mathbf{x}_i$ , and the coarse interval  $\mathcal{T}_i$ , estimate the  $i$ th crossing point  $\tau_i$  of  $s(t)$  and  $y(t)$ . As illustrated in Fig. 2 for a sawtooth carrier, this problem is tantamount to interpolating through the  $M$  noisy samples contained in vector  $\mathbf{x}_i$  in (4). In this respect,  $M - 1$  represents the interpolation order while for a given  $M$ ,  $M_1$  controls the offset applied to the interpolation window, allowing for a low-delay estimate even with large  $M$ . The trade-offs in the choice of  $M$  and  $M_1$  are explored in Section 5. Note that using  $M > 2$  makes it possible to correct local errors in the coarse interval estimate obtained by  $E_1$ .

Finally, we consider the following general model for the periodic carrier signal, which is applicable to various types of PWM:

$$y(t) = Y_{dc} + A_c \sum_i \varepsilon^i p(t - iT_c), \quad (5)$$

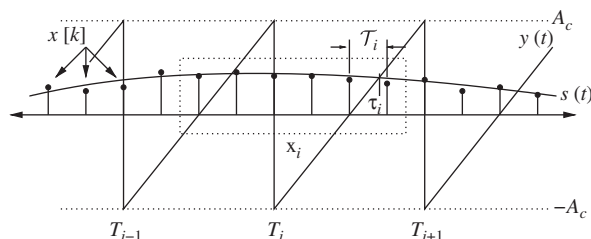


Fig. 2. Forming the sample vector  $\mathbf{x}_i$ :  $M=6$ ,  $M_1=5$  and  $M_2=1$ . The sample vector is shown in the dashed box.

where  $Y_{dc}$  is a dc offset,  $A_c > 0$  is a positive gain,  $i \in \mathbb{Z}$  is the pulse index,  $\varepsilon \in \{-1, 1\}$  controls the pulse polarity,  $T_c$  is the pulse duration and  $p(t)$  is the basic pulse shape. The latter is expressed as

$$p(t) = \begin{cases} \phi(t), & 0 \leq t \leq T_c, \\ 0 & \text{otherwise} \end{cases} \quad (6)$$

for some real-valued function  $\phi(t)$ . We denote the  $i$ th basic pulse interval as

$$C_i \triangleq (T_i, T_{i+1}), \quad (7)$$

where  $T_i = iT_c$ . The standard single-edge PWM carrier is a special case of (5)–(6), obtained by setting  $Y_{dc} = 0$ ,  $\varepsilon = 1$ ,  $\phi(t) = (2t - T_c)/T_c$  (i.e. a ramp) and  $T_c = T_s$ ; the standard double-edge PWM carrier is obtained from the above by using  $\varepsilon = -1$  instead (see e.g. [15]). Other types of carrier waveforms (e.g. sinusoidal) can be obtained by a suitable choice of the model parameters and the function  $\phi(t)$ . In this work, we set  $Y_{dc} = 0$  without loss in generality and make the following practical assumptions:

- A1. The function  $\phi(t)$  is continuous and increasing from  $-1$  to  $+1$  on the interval  $0 < t < T_c$ , i.e.:  $\phi(0^+) = -1$ ,  $\phi(T_c^-) = +1$  and  $\phi'(t) > 0$ . This ensures that  $y(t)$  is one-to-one in every pulse interval  $C_i$ .
- A2. The peak amplitude  $A_c$  is sufficiently large so that the probability of dynamic overflow, i.e.  $|s(t)| > A_c$ , is negligible. This ensures that there is at least one crossing point within each pulse interval  $C_i$ .
- A3. The rate of change of the carrier signal  $y(t)$  within a basic pulse period, as measured by e.g. the ratio  $2A_c/T_c$ , is sufficiently large to ensure that only a single crossing point occurs in every interval  $C_i$ .
- A4. The sampling frequency is commensurate with the pulse repetition rate [15], i.e.  $T_c = \eta T_s$  for some integer  $\eta \geq 1$ .

These assumptions, which reflect normal operating conditions for switched circuit modulations (i.e. no overload), greatly simplify the derivation and analysis of optimum crossing-point estimators in the following sections.

### 3. Algorithm development

We now focus on  $E_2$  and develop optimal estimators for  $\tau_i$  by exploiting statistical knowledge about the input vector  $\mathbf{x}_i$ . Since we only need to consider a single crossing point at a time, we may drop the subscript  $i$  on  $\tau_i$ ,  $\mathcal{T}_i$  and  $\mathbf{x}_i$  without ambiguity.

#### 3.1. Probability distribution of sample vectors

Consider the  $M$ -dimensional observation vector  $\mathbf{x} \equiv \mathbf{x}_i$  in (4), whose entries are obtained from consecutive samples of  $x[k]$  in (1). We can write

$$\mathbf{x} = \mathbf{s} + \mathbf{n}, \quad (8)$$

where we define the  $M$ -dimensional signal and noise vectors,  $\mathbf{s}$  and  $\mathbf{n}$ , respectively, as follows ( $M = M_1 + M_2$ ):

$$\mathbf{s} \triangleq \begin{bmatrix} s[(k-M_1)T_s] \\ \vdots \\ s[(k+M_2-1)T_s] \end{bmatrix}, \quad \mathbf{n} \triangleq \begin{bmatrix} n[k-M_1] \\ \vdots \\ n[k+M_2-1] \end{bmatrix}. \quad (9)$$

Under the modeling assumptions in Section 2.1,  $\mathbf{x}$  has zero mean, i.e.  $E\{\mathbf{x}\} = 0$ , and its covariance matrix  $\Sigma_x \triangleq E\{\mathbf{x}\mathbf{x}^T\}$ , of size  $M \times M$ , is given by

$$\Sigma_x = \Sigma_s + \Sigma_n, \quad (10)$$

where  $\Sigma_s \triangleq E\{\mathbf{s}\mathbf{s}^T\}$  and  $\Sigma_n \triangleq E\{\mathbf{n}\mathbf{n}^T\}$  are the covariance matrices of the signal and noise components, respectively. These can be expressed as

$$\Sigma_s \triangleq \text{Toep}[\sigma_s^2, r_s(T_s), \dots, r_s((M-1)T_s)], \quad (11)$$

$$\Sigma_n \triangleq \text{Toep}[\sigma_n^2, r_n[1], \dots, r_n[M-1]], \quad (12)$$

where  $\text{Toep}[a_0, a_1, \dots, a_{M-1}]$  denotes a symmetric Toeplitz matrix with the vector  $[a_0, a_1, \dots, a_{M-1}]$  as its first row. We assume that  $\Sigma_s$  and  $\Sigma_n$  are positive definite and therefore invertible.

Since  $s(t)$  is modeled as a Gaussian process, the signal vector  $\mathbf{s}$  in (9) has a multi-variate Gaussian distribution. To determine the probability distribution of the observation vector  $\mathbf{x}$  in (8), we need to examine the statistical properties of the noise component. We consider two cases of interest.

In systems operating at low SNR (i.e. small number of bits), a noise shaping stage can be employed prior to the crossing-point estimation to move quantization noise outside the band of interest [31]. In this case, as explained in Section 2, the filtered noise is usually modeled as a Gaussian process and the observation vector  $\mathbf{x}$ , which is then the sum of two independent Gaussian components, admits a multi-variate Gaussian distribution.

In systems operating at high SNR without noise shaping, the noise samples cannot be assumed Gaussian; in this case, the standard model is the uniform distribution. We note however that the probability density function (pdf) of  $\mathbf{x}$ , say  $f_{\mathbf{x}}(\xi)$ , is given by the (multi-dimensional) convolution of the signal pdf,  $f_s(\xi)$ , with the noise pdf,  $f_n(\xi)$  [37]. At high SNR, the noise pdf is concentrated around the origin and the convolution only has a local smoothing effect on the signal pdf. Hence, we expect that the multi-variate Gaussian shape of  $f_s(\xi)$  is nearly preserved in the resulting pdf  $f_{\mathbf{x}}(\xi)$ .

These observations are theoretically supported by the following proposition which covers both cases of interest.

**Proposition 1.** *The pdf of the observation vector  $\mathbf{x}$  in (8) admits an asymptotic expansion:*

$$f_{\mathbf{x}}(\xi) = \frac{1}{(2\pi)^{M/2} |\Sigma_x|^{1/2}} e^{-(1/2)\xi^T \Sigma_x^{-1} \xi} + \mathcal{O}\left(\frac{\sigma_n^3}{\sigma_x^3} \kappa_{k_1 \dots k_M}^{(3)}\right), \quad (13)$$

where  $\sigma_x^2 \triangleq \sigma_s^2 + \sigma_n^2$ ,  $|\Sigma_x|$  denotes the determinant of  $\Sigma_x$ , and  $\kappa_{k_1 \dots k_M}^{(v)}$  are the cumulants of order  $v$  of the normalized noise vector  $\sigma_n^{-1} \mathbf{n}$ .

A proof of this general property is given in Appendix A. Relation (13) provides an asymptotic expansion for the pdf of  $\mathbf{x}$  as the sum of a dominant multi-variate Gaussian

pdf and small correction terms in  $(\sigma_n^v / \sigma_x^v) \kappa_{k_1 \dots k_M}^{(v)}$ , with the first such correction beginning at  $v = 3$ . The presence of cumulants of order 3 and beyond accounts for a possible deviation of the noise vector's pdf from the Gaussian distribution. When the noise is Gaussian, these cumulants are zero and only the dominant multi-variate Gaussian term remains in (13). When the noise is not Gaussian but the SNR is high, the correction terms in (13) will be small in general. For example, for an SNR of 10 dB, which is on the very low side for the current application, we have  $\sigma_n^3 / \sigma_x^3 \approx 0.03$ . If in addition the 3rd order cumulants are zero, which is the case with uniformly distributed quantization noise, the first correction term is in  $\sigma_n^4 / \sigma_x^4 < 0.01$ .

In this work, it is therefore well justified to assume that the observation vector  $\mathbf{x}$  can be modeled by a multi-variate Gaussian distribution, i.e.:

$$f_{\mathbf{x}}(\xi) = \frac{1}{(2\pi)^{M/2} |\Sigma_x|^{1/2}} e^{-(1/2)\xi^T \Sigma_x^{-1} \xi}. \quad (14)$$

### 3.2. Maximum a posteriori (MAP) estimation

We model the unknown crossing point  $\tau$  as a random variable with *a priori* pdf  $f_{\tau}(t)$ . We denote the conditional pdf of  $\tau$  given a particular realization of the observation vector, i.e.  $\mathbf{x} = \xi$ , as  $f_{\tau|\mathbf{x}}(t|\xi)$ . By definition, the MAP estimate of  $\tau$  given  $\mathbf{x} = \xi$  maximizes this latter function, i.e.

$$\hat{\tau}_{\text{MAP}} = \underset{t \in \Theta}{\text{argmax}} f_{\tau|\mathbf{x}}(t|\xi), \quad (15)$$

where  $\Theta$  denotes the search interval, whose choice is discussed below. To solve for  $\hat{\tau}_{\text{MAP}}$ , we begin with the canonical MAP equation [38]:

$$\left( \frac{d}{dt} \log f_{\mathbf{x}|\tau}(\xi|t) + \frac{d}{dt} \log f_{\tau}(t) \right) \Big|_{t = \hat{\tau}_{\text{MAP}}} = 0, \quad (16)$$

where  $f_{\mathbf{x}|\tau}(\xi|t)$  is the conditional pdf of  $\mathbf{x}$  given a crossing point at  $\tau = t$ .

#### 3.2.1. A priori pdf of a crossing point

The choice of the search interval  $\Theta$  and the *a priori* pdf  $f_{\tau}(t)$  depends on properties of the coarse estimator  $E_1$  and related system parameters. Two cases of interest are considered below.

*Case 1:* The situation in which the search interval corresponds to the basic pulse duration, i.e.  $\Theta = C_i$  in (7), is of primary importance. It occurs for instance in standard single-edge and double-edge PWM, where by design  $T_s = T_c$  and a single crossing point per sample is guaranteed. In the absence of additional information, the crossing time may occur anywhere within  $\Theta$  with a pdf  $f_{\tau}(t)$  that can be derived as follows.

Consider a *rising* segment  $C_i$  of the carrier  $y(t)$  over the interval  $C_i$ , as illustrated in Fig. 2 for a sawtooth waveform. We first note that under assumptions A1–A4 in Section 2, the condition  $\tau \leq t \in C_i$  on the crossing point is **equivalent** to the condition  $s(t) \leq y(t)$  between the input and carrier signals. That is, for a rising carrier and assuming a single crossing point within  $C_i$ , this crossing point occurs at time  $\tau \leq t$  if and only if the value of the comparison waveform

at time  $t$ ,  $y(t)$ , exceeds that of the input,  $s(t)$ . Therefore, we can write

$$F_\tau(t) \triangleq \Pr\{\tau \leq t\} = \Pr\{s(t) \leq y(t)\}, \quad t \in \Theta, \quad (17)$$

where  $F_\tau(t)$  denotes the cumulative distribution function of  $\tau$ . Since by assumption  $s(t)$  is zero mean Gaussian with variance  $\sigma_s^2$ , we have

$$F_\tau(t) = \int_{-\infty}^{y(t)} \frac{1}{\sqrt{2\pi\sigma_s^2}} e^{-(1/2\sigma_s^2)u^2} du, \quad t \in \Theta.$$

Differentiating with respect to  $t$ , we finally obtain the desired pdf:

$$f_\tau(t) = \frac{1}{\sqrt{2\pi\sigma_s^2}} e^{-(1/2\sigma_s^2)y(t)^2} |\dot{y}(t)|, \quad t \in \Theta, \quad (18)$$

where the dot notation is used to express differentiation with respect to  $t$ , i.e.  $\dot{y}(t) \equiv (d/dt)y(t)$ . Since the search is limited to the open interval  $\Theta = C_i$  where the pulse waveform  $p(t - iT_c)$  is smooth, we do not need to take into consideration the possible singularities of  $\dot{y}(t)$  at the end points of the pulse period. The case of a falling segment can be treated in a similar way; it is accounted for by the presence of the absolute value in (18).

*Case 2:* Another situation of interest is when  $T_c = \eta T_s$  with  $\eta \geq 2$  and the coarse estimator  $E_1$  is sufficiently reliable. In this case, the search interval can generally be restricted to a proper subset  $\Theta \subset C_i$ . This may range from a single sampling interval when the output of  $E_1$  is error-free, i.e.  $\Theta = \mathcal{T}_i(4)$ , to a few sampling intervals otherwise, in which case  $\Theta \supset \mathcal{T}_i$ . Note that by extending the search region beyond the coarse interval  $\mathcal{T}_i$ , the refined estimator  $E_2$  is in effect allowed to correct possible errors in the output of  $E_1$ . While the approach used in Case 1 to develop  $f_\tau(t)$  can be extended to this case as well, it may be more appropriate here to design  $f_\tau(t)$  based on *a priori* knowledge of the distribution of the coarse estimation errors. If this information is not available, a uniform distribution can be used instead.

### 3.2.2. Conditional pdf of the observations

We next derive an expression for  $f_{\mathbf{x}|\tau}(\xi|t)$ , the conditional pdf of observation vector  $\mathbf{x}$  given a crossing point at  $\tau = t$ . To this end, we first introduce an augmented  $(M+1) \times 1$  random vector, defined as

$$\bar{\mathbf{x}} = \begin{bmatrix} \mathbf{x} \\ s(t) \end{bmatrix} = \begin{bmatrix} \mathbf{s} \\ s(t) \end{bmatrix} + \begin{bmatrix} \mathbf{n} \\ 0 \end{bmatrix}. \quad (19)$$

Invoking Proposition 1, we assume as before that  $\bar{\mathbf{x}}$  is a Gaussian random vector with zero mean and covariance matrix denoted as  $\bar{\Sigma}$ . The latter may be expressed in partitioned form as follows:

$$\bar{\Sigma} = \begin{bmatrix} \Sigma_x & \boldsymbol{\rho}(t) \\ \boldsymbol{\rho}(t)^T & \sigma_s^2 \end{bmatrix}, \quad (20)$$

where we define

$$\boldsymbol{\rho}(t) \triangleq \begin{bmatrix} r_s(t - [k - M_1]T_s) \\ \vdots \\ r_s(t - [k + M_2 - 1]T_s) \end{bmatrix}.$$

We now make the following key observation: conditioning on a crossing point at time  $\tau = t$  is equivalent to conditioning on the event  $s(t) = y(t)$ , i.e. assuming a known value of  $y(t)$  for the last entry of the augmented vector  $\bar{\mathbf{x}}$  in (19). Using well-known properties of the multivariate Gaussian distribution [39], it follows that  $f_{\mathbf{x}|\tau}(\xi, t)$  is also multi-variate Gaussian with covariance matrix  $\Sigma(t)$  and mean  $\boldsymbol{\mu}(t)$ , respectively, given by

$$\Sigma(t) = \Sigma_x - \frac{1}{\sigma_s^2} \boldsymbol{\rho}(t) \boldsymbol{\rho}(t)^T, \quad (21)$$

$$\boldsymbol{\mu}(t) = \frac{1}{\sigma_s^2} y(t) \boldsymbol{\rho}(t). \quad (22)$$

Therefore, we finally obtain

$$f_{\mathbf{x}|\tau}(\xi|t) = \frac{1}{(2\pi)^{M/2} |\Sigma(t)|^{1/2}} e^{-(1/2)(\xi - \boldsymbol{\mu}(t))^T \Sigma(t)^{-1} (\xi - \boldsymbol{\mu}(t))}. \quad (23)$$

### 3.2.3. The MAP estimator

The MAP estimate of  $\tau$  satisfies (16). Based on our discussion in Section 3.2.1, different cases are possible for the term  $(d/dt)\log f_\tau(t)$ . Under Case 1 and assuming a rising segment (i.e.  $\dot{y}(t) > 0$  for all  $t \in C_i$ ), we find

$$\frac{d}{dt} \log f_\tau(t) = \frac{\dot{y}(t)}{y(t)} - \frac{\dot{y}(t)y(t)}{\sigma_s^2}. \quad (24)$$

We note that as a consequence of assumption A2, the evaluation of the derivatives of  $y(t)$  in (24) is limited to interior points of the basic pulse interval  $C_i \triangleq (T_i, T_{i+1})$ . Consequently, these derivatives are well defined and we do not have to worry about possible singularities at end-points  $T_i$  and  $T_{i+1}$  (see Fig. 1). Under Case 2, the choice of  $f_\tau(t)$  will reflect the distribution of the coarse estimation errors. If this information is not available and a uniform distribution is used instead, we have

$$\frac{d}{dt} \log f_\tau(t) = 0 \quad (25)$$

for all interior points  $t \in \Theta$ . When applied to (16), the resulting estimator is then equivalent to a maximum likelihood (ML) estimator.

Using (23), the term  $(d/dt)\log f_{\mathbf{x}|\tau}(\xi|t)$  in (16) can be expressed as

$$\frac{d}{dt} \log f_{\mathbf{x}|\tau}(\xi|t) = -\frac{1}{2} \frac{d}{dt} (\log |\Sigma(t)| + (\xi - \boldsymbol{\mu}(t))^T \Sigma(t)^{-1} (\xi - \boldsymbol{\mu}(t))). \quad (26)$$

Applying the Sherman–Morrison–Woodbury formula [40] to (21), we may express  $\Sigma(t)^{-1}$  in terms of  $\Sigma_x^{-1}$ :

$$\Sigma(t)^{-1} = \Sigma_x^{-1} + \frac{\Sigma_x^{-1} \boldsymbol{\rho}(t) \boldsymbol{\rho}(t)^T \Sigma_x^{-1}}{\sigma_s^2 - \boldsymbol{\rho}(t)^T \Sigma_x^{-1} \boldsymbol{\rho}(t)}. \quad (27)$$

This formula is valid provided that  $\Sigma_x$  is nonsingular, which is always true in the presence of noise (i.e.  $\sigma_n^2 > 0$ ). Next, we define the following quantities, whose dependence on  $t$  is omitted to simplify the notations:

$$\begin{aligned} a_0 &= \boldsymbol{\rho}(t)^T \Sigma_x^{-1} \boldsymbol{\rho}(t) / \sigma_s^2, & c_0 &= \boldsymbol{\xi}^T \Sigma_x^{-1} \boldsymbol{\rho}(t), \\ b_0 &= \boldsymbol{\rho}(t)^T \Sigma_x^{-1} \dot{\boldsymbol{\rho}}(t) / \sigma_s^2, & d_0 &= \boldsymbol{\xi}^T \Sigma_x^{-1} \dot{\boldsymbol{\rho}}(t), \\ e_0 &= \dot{\boldsymbol{\rho}}(t)^T \Sigma_x^{-1} \dot{\boldsymbol{\rho}}(t) / \sigma_s^2. \end{aligned} \quad (28)$$

Substituting (27) in (26) and using (28), we obtain

$$\frac{d}{dt} \log f_{\mathbf{x}|\tau}(\xi|t) = -\frac{b_0(a_0 y - c_0)(y - c_0)}{\sigma_s^2(1 - a_0)^2} + \frac{d_0 y}{\sigma_s^2} + \frac{b_0 \sigma_s^2 + (d_0 - y)(a_0 y - c_0) - b_0 y(y - c_0)}{\sigma_s^2(1 - a_0)} \quad (29)$$

This completes the derivation. The MAP estimate satisfies (16), where the first term on the LHS is given by (29) and the second term can be taken as (24) or (25). To generate estimates using this expression, a zero-finding method such as Brent's algorithm [41] or Newton's method may be applied. There is no guarantee that a unique zero of (16) exists in the search interval  $\Theta$ , and that it corresponds to the absolute maximum of  $f_{\mathbf{x}|\tau}(\xi|t)$  within  $\Theta$ . We do not investigate uniqueness of the solution in this work; our experimental results suggest that it is not a critical issue.

### 3.3. Minimum mean squared error formulation

Estimators using (29) can be numerically sensitive and expensive. Here, we introduce a simpler crossing-point estimator based on minimum mean squared error (MMSE) interpolation. This estimator is shown to be an approximation to the MAP estimator under appropriate conditions.

Let  $\hat{s}_o(t, \xi)$  denote the MMSE estimator of  $s(t)$  at arbitrary time  $t$ , given a realization  $\mathbf{x} = \xi$  of the observation vector. According to the Wiener–Hopf equation [42], this estimator can be expressed in the form

$$\hat{s}_o(t, \xi) = \boldsymbol{\rho}(t)^T \Sigma_x^{-1} \xi = c_0, \quad (30)$$

where  $c_0 \equiv c_0(t, \xi)$  in defined in (28). The corresponding MMSE is given by

$$\varepsilon = \sigma_s^2 - \boldsymbol{\rho}(t)^T \Sigma_x^{-1} \boldsymbol{\rho}(t) = \sigma_s^2(1 - a_0), \quad (31)$$

where it can be verified that  $0 \leq \varepsilon \leq \sigma_s^2$ . We may consider  $\varepsilon$  to provide a measure of confidence in  $\hat{s}_o(t, \xi)$ . In particular, when  $\mathbf{x}$  consists of closely spaced samples near  $t$  and the measurement noise is small,  $\varepsilon$  will be small compared to  $\sigma_s^2$ , or equivalently,  $0 \leq 1 - a_0 \ll 1$  over the region of interest.

In such a case, the first term on the right-hand side of (29) will dominate the others, resulting in the approximation:

$$\frac{d}{dt} \log f_{\mathbf{x}|\tau}(\xi|t) \simeq \frac{b_0(y - c_0)^2}{\sigma_s^2(1 - a_0)^2}. \quad (32)$$

The MMSE (or approximated MAP) estimate corresponds to the zeros of (32). The two candidates are roots of  $b_0$  and  $y - c_0$ . However, as  $b_0$  is a function of  $t$  and  $\Sigma_x^{-1}$  only, it does not involve the sample vector in any way. Choosing the roots of the remaining term results in an estimator which performs well and is intuitively satisfying.

Define the  $M$ -dimensional weight vector  $\mathbf{w}_o = \Sigma_x^{-1} \xi$ . The MMSE-based estimate of the crossing point must satisfy the following relation:

$$\hat{s}_o(t, \xi) = \mathbf{w}_o^T \boldsymbol{\rho}(t) = y(t). \quad (33)$$

We denote this estimate as  $\hat{\tau}_{\text{MMSE}}$ , i.e.:

$$(\mathbf{w}_o^T \boldsymbol{\rho}(t) - y(t))|_{t = \hat{\tau}_{\text{MMSE}}} = 0. \quad (34)$$

This result has an intuitive form, since it relates the MMSE estimate of  $s(t)$  to the carrier signal and solves for the points at which they are equal. Since both the carrier signal and  $\boldsymbol{\rho}(t)$  are in general nonlinear functions, a root-finding method must be adopted. Similar to the MAP estimator, we assume the existence and uniqueness of solutions to (34) over the search interval  $\Theta$ .

### 3.4. Summary of algorithms

The computational structure of the MAP and MMSE estimators is summarized in Algorithm 1. The only difference between the two estimators is in the choice of the score function  $g(t)$  used in the root-solving step, i.e. LHS of (16) for the MAP versus LHS of (34) for the MMSE. We note that the computational difficulties in the MAP estimator do not occur with the MMSE, and a simple zero-finding algorithm performs well. Indeed, we use the MMSE estimate as an initial guess to the MAP estimate in our experiments.

**Algorithm 1.** Crossing-point estimation via MAP or MMSE

```

select:  $g(t) \leftarrow (16)$  for MAP;  $g(t) \leftarrow (34)$  for MMSE
loop
  if  $\tau \in \mathcal{T}_i$  then
     $\xi = [x[k_i - M_1], \dots, x[k_i + M_2 - 1]]^T$ 
     $\mathbf{w}_o = \Sigma_x^{-1} \xi$  (using Cholesky factorization of  $\Sigma_x^{-1}$ )
     $\hat{\tau}_0 =$  initial estimate of crossing point
    repeat
       $\hat{\tau}_k =$  refine  $\hat{\tau}_{k-1}$  using Newton's or Brent's algorithm applied to  $g(t)$ .
       $\delta = |g(\hat{\tau}_k)|$ 
    until  $\delta < \text{tol}$ 
    end if
  end loop

```

## 4. Performance considerations

### 4.1. Bound on crossing-point estimator MSE

The Bayesian Cramér–Rao bound (CRB) provides a lower bound on the attainable MSE of any estimator  $\hat{\tau}(\mathbf{x})$  of  $\tau$  as follows [38,43]:

$$E\{[\hat{\tau}(\mathbf{x}) - \tau]^2\} \geq \frac{1}{E\{\mathcal{I}(\tau)\} + \mathcal{I}_o}. \quad (35)$$

The denominator on the RHS of (35), referred to as the Bayesian information, is the sum of two terms which, respectively, depend on the conditional pdf of the observation vector,  $f_{\mathbf{x}|\tau}(\xi|t)$ , and the *a priori* pdf of the crossing point,  $f_\tau(t)$ . In this respect, the Bayesian CRB is a fundamental property of these two pdfs, irrespective of any specific estimator  $\hat{\tau}(\mathbf{x})$ . The computation of the terms  $E\{\mathcal{I}(\tau)\}$  and  $\mathcal{I}_o$  is further discussed below.

The function  $\mathcal{I}(\cdot)$  appearing in (35) is the so-called Fisher information of the conditional pdf  $f_{\mathbf{x}|\tau}(\xi|t)$ , defined as the following multi-dimensional conditional expectation [44]:

$$\mathcal{I}(t) = \int \dots \int \left( \frac{\partial \log f_{\mathbf{x}|\tau}(\xi|t)}{\partial t} \right)^2 f_{\mathbf{x}|\tau}(\xi|t) d\xi_1 \dots d\xi_M. \quad (36)$$

For the problem under consideration here, i.e. with the special form of  $f_{\mathbf{x}|\tau}(\xi|t)$  in (23), the Fisher information takes the following form [45]:

$$\mathcal{I}(t) = \dot{\boldsymbol{\mu}}^T \Sigma^{-1} \dot{\boldsymbol{\mu}} + \frac{1}{2} \text{tr}[\Sigma^{-1} \dot{\Sigma} \Sigma^{-1} \dot{\Sigma}], \quad (37)$$

where the dependence of  $\boldsymbol{\mu}$  and  $\Sigma$  on  $t$  is omitted for convenience. This expression may readily be simplified using the notation introduced in (28):

$$\mathcal{I}(t) = \frac{b_0^2(1+a_0)}{(1-a_0)^2} + \frac{b_0^2 y^2 + 2b_0 y \dot{y} + a_0 \dot{y}^2}{\sigma_s^2(1-a_0)} + \frac{a_0 e_0}{1-a_0} + \frac{e_0 y^2}{\sigma_s^2}, \quad (38)$$

where again, we recall that  $a_0, b_0, e_0$  and  $y$  are functions of  $t$ .

To remove the effect of specific realizations of the crossing point  $\tau$ , the Bayesian CRB in (35) further averages the Fisher information over permissible values of this random variable. In the situation of interest here, *a priori* knowledge is available about the unknown crossing-point location  $\tau$  in two forms: first, we have a coarse location furnished by estimator  $E_1$  (see Fig. 1) and represented by the search interval  $\Theta$ ; second, we have an *a priori* crossing-point pdf  $f_\tau(t)$ , as in e.g. (18). Accordingly, we may use

$$E\{\mathcal{I}(\tau)\} = \int_{\Theta} \mathcal{I}(t) f_\tau(t) dt. \quad (39)$$

Finally, the quantity  $\mathcal{I}_o$  in (35) is the Fisher information of the *a priori* pdf of the crossing point,  $f_\tau(t)$ , and is given by

$$\mathcal{I}_o = \int_{\Theta} \left( \frac{d}{dt} \ln f_\tau(t) \right)^2 f_\tau(t) dt. \quad (40)$$

As explained in Section 3.2.1, the search interval  $\Theta$  and the *a priori* pdf  $f_\tau(t)$  depend on the specific carrier signal  $y(t)$  and associated system parameters. For a given choice of  $\Theta$  and  $f_\tau(t)$ , the Bayesian CRB can be evaluated via numerical integration of (39) and (40), where in the former, expression (38) of the Fisher information is used. This bound will be used as a benchmark for comparison of estimator MSE in our simulation study.

A simplified expression for the Bayesian CRB can be obtained under the condition of high SNR in the oversampled regime. Indeed, proceeding as in Section 3.3 and assuming that the MMSE (31) is small over the search interval  $\Theta$ , we can approximate the Fisher information (38) as

$$\mathcal{I}(t) \simeq \frac{2b_0^2}{(1-a_0)^2} = \frac{2\sigma_s^2 [\boldsymbol{\rho}(t)^T \Sigma_x^{-1} \boldsymbol{\rho}(t)]^2}{\sigma_s^2 - \boldsymbol{\rho}(t)^T \Sigma_x^{-1} \boldsymbol{\rho}(t)}. \quad (41)$$

The desired simplified expression for the CRB (35) follows upon substitution of the above approximation in (39).

## 4.2. Computational complexity

The complexity of a crossing-point estimation method is an important consideration. For switching audio amplifiers in particular, crossing points must be calculated at a rate of several hundred kHz or more. Here, we briefly discuss the computational complexity of the above optimum estimators where for simplicity, a cost of 1 corresponds to any basic mathematical operation (addition, multiplication, comparison, etc.) available on the implementing technology. We let  $\nu$  denote the cost of evaluating a scalar nonlinear function. For example, the costs for  $y(\tau)$  and  $\boldsymbol{\rho}(\tau)$  are  $\nu$  and  $M\nu$ , respectively.

The proposed estimators share a similar structure. First, each crossing point  $\tau$  is coarsely located using estimator  $E_1$ . This process contributes a cost of  $(\nu+1)$  per sample, i.e.: evaluation of the carrier function and comparison to the observed sample at the rate  $1/T_s$ . Alternatively, depending on the available hardware, a table look-up approach can be used to store the values of  $y(nT_s)$ ; in this case, only comparisons are needed. Next, samples in the neighborhood of  $\mathcal{T}_i$  are passed to  $E_2$  to generate a refined estimate. For each scheme, this is achieved using an iterative root-finding process such as Brent's method [41]; here, we let  $k$  denote the average number of required iterations. Referring to Algorithm 1, the Cholesky factorization of  $\Sigma_x^{-1} = LL^T$  can be precomputed. Therefore, we may compute the vector  $\mathbf{w}_o = \Sigma^{-1} \boldsymbol{\xi}$  by forward-backward substitution at a total cost of  $2M^2$ .

Beginning with the MMSE estimator, the cost of evaluating the LHS in (34) is  $(M+1)\nu+2M$ . Therefore, the required number of floating-point operations per unit sampling period for this estimator may be expressed as

$$C_{\text{MMSE}} = \nu + 1 + \frac{1}{\eta} (2M^2 + k[(M+1)\nu + 2M]), \quad (42)$$

where  $\eta = T_c/T_s$ . For the MAP estimator, we proceed in the same way but we also need to take into account the calculation of the various time dependent quantities in (28). The total required number of floating-point operations per unit sampling period for this estimator is

$$C_{\text{MAP}} = \nu + 1 + \frac{1}{\eta} (2M^2 + k[2M^2 + 2(M+1)\nu + 8M + 16]). \quad (43)$$

For comparison purposes, we also consider a traditional crossing-point estimator based on Lagrange polynomial interpolation of order  $M$  (see Section 5 for details). The computational cost of this estimator can be expressed as

$$C_{\text{POL}} = \nu + 1 + \frac{k}{\eta} [(M+1)\nu + 2M]. \quad (44)$$

## 5. Simulation experiments

In this section, we present simulation experiments in which the performance of the proposed methods is evaluated and characterized as a function of various system parameters.

### 5.1. Methodology

We consider a PWM application and explore the influence of the system and signal parameters in Table 1. With the exception of  $f_m$ , which corresponds to the (strict) bandlimit of  $s(t)$ , these parameters have been introduced in previous sections. The values in this table are nominal values which we alter individually. We have chosen a high SNR  $\triangleq \sigma_s^2 / \sigma_n^2$  of approximately 83 dB, which is representative of high-quality digital audio sources with 16 bit word length. We let  $y(t)$  be a sawtooth periodic waveform with amplitude  $A_c=1$  and pulse repetition frequency  $f_c=2f_m$ , which corresponds to the signal's Nyquist rate. In practice,

**Table 1**  
Nominal values of system parameters in experimental study.

Parameter	Value	Description
$f_s = 1/T_s$	192 kHz	Sampling rate
$f_m$	24 kHz	Bandlimit of $s(t)$
$f_c = 1/T_c$	48 kHz	Pulse repetition rate
$M = 2M_1$	4	Number of samples
$A_c$	1	Carrier amplitude
$\sigma_n^2$	$2^{-30}/12$	Noise variance
$\sigma_s^2$	$(1/8)^2$	Signal variance

PWM implementations may use a carrier frequency of several times this value.

We model  $s(t)$  as a wide-sense stationary Gaussian random process with zero mean and flat, bandlimited power spectral density (psd), i.e.:

$$P_s(\omega) = \begin{cases} \pi\sigma_s^2/\Omega_m, & |\omega| < \Omega_m, \\ 0 & \text{otherwise.} \end{cases} \quad (45)$$

The autocorrelation function of  $s(t)$  may be expressed as [37]

$$r_s(t) = \sigma_s^2 \text{sinc}(\Omega_m t/\pi), \quad (46)$$

where  $\Omega_m = 2\pi f_m$ . This expression for  $r_s(t)$  is used to evaluate the vector  $\rho(\tau)$  within the MAP and MMSE estimators.

During the simulations, in addition to the samples of  $s(t)$  needed to form the vectors  $\mathbf{x}$ , we require precise knowledge of each of the true crossing points of  $s(t)$  and  $y(t)$  in order to evaluate the error for each estimator. To determine these crossing points with high precision, it is necessary to generate  $s(t)$  in such a way that it may be evaluated at arbitrary time instants with a low computational cost. To this end, we use the following synthesis model:

$$s(t) = \sum_{n=1}^N \sqrt{2\sigma_s^2/N} \sin(\omega_n t + \phi_n), \quad t_0 \leq t \leq t_{M-1}, \quad (47)$$

where  $\omega_n$  and  $\phi_n$  ( $n=1, \dots, N$ ) are independent, uniformly distributed random variables over the intervals  $[0, \Omega_m]$  and  $[0, 2\pi)$ , respectively. We use  $N=10$  terms in the summation to properly approximate the desired PSD (46). We have found this approach to give similar results to a Karhunen–Loève expansion using prolate spheroidal wave functions [46,38], but much lower complexity; additional details can be found in [47].

### 5.1.1. Monte Carlo simulations

For each independent experimental trial, the frequency and phase parameters of  $s(t)$  (47) are generated randomly. Knowledge of these parameters allows precise evaluation of  $s(t)$  at any point within the observation interval, taken to be  $[-M_1 T_s, T_c + M_2 T_s - 1]$ . Signal  $s(t)$  is then sampled, and uniformly distributed noise is added to form the sequence  $x[k]$  in (1).

Coarse estimation of the crossing point is performed by monitoring the sign of  $d[k]$  (2) over the pulse period of interest, i.e.  $C_0 = [0, T_c]$ . Samples of  $x[k]$  surrounding the

coarse estimate are combined into vector  $\xi$ , as per Algorithm 1. A refined estimate is then computed by feeding  $\xi$  into one of several methods as described below. Estimates that fall outside the search interval  $\Theta = C_0$  are handled as follows: if  $\hat{\tau} > T_c$ , set  $\hat{\tau} = T_c$ ; if  $\hat{\tau} < 0$ , set  $\hat{\tau} = 0$ . To ensure statistical reliability, each data point on the graphs in Section 5.2 represents an ensemble average over  $\geq 2000$  independent trials.

For each trial, we compute the proposed MAP, using the *a priori* pdf  $f_\tau(t)$  (18), and MMSE estimators. For comparison purposes, we also compute two estimators based on polynomial interpolation, namely: Lagrange and cubic spline. While polynomial interpolation may be sensitive to noise (especially colored noise), it is widely applied to the crossing-point problem because of its low complexity, as discussed earlier. We adopt a vector formulation for Lagrange interpolation [48–50]. Define the vector function  $\mathbf{l}(t) = [l_0(t), \dots, l_{M-1}(t)]^T$  componentwise as follows:

$$l_m(t) = \prod_{\substack{n=k_1-M_1 \\ n \neq m}}^{k_1+M_2-1} \frac{t-nT_s-T_d}{(m-n)T_s}, \quad m=0, \dots, M-1. \quad (48)$$

Given the vector of noisy samples  $\xi$ , a polynomial approximation of degree  $M-1$  of  $s(t)$  is then obtained via the inner product  $\xi^T \mathbf{l}(t)$ . The resulting crossing-point estimate, denoted  $\hat{\tau}_{\text{POL}}$ , is defined as

$$(\xi^T \mathbf{l}(t) - y(t))|_{t=\hat{\tau}_{\text{POL}}} = 0. \quad (49)$$

In the case  $M=2$ , the POL estimator forms a straight line between  $x[k_i - 1]$  and  $x[k_i]$  and determines the time at which it crosses  $y(t)$ . We consider this special case because it is in general treated separately from higher-order polynomial methods in the literature, and since its solution may be expressed in closed form without recourse to root-finding when  $y(t)$  is a sawtooth carrier. We explicitly refer to the resulting estimate as  $\hat{\tau}_{\text{LIN}}$ . We also consider a standard cubic spline interpolator for comparison; the defining equations can be found in [51]. The resulting crossing-point estimate is denoted as  $\hat{\tau}_{\text{SPL}}$ .

As a performance benchmark, we evaluate the Bayesian CRB (35) on the minimum achievable MSE, using the *a priori* pdf  $f_\tau(t)$  (18) in (39)–(40). As a worst case performance, we also consider the variance of a uniformly distributed random variable within the coarse interval (3). The corresponding value of  $T_s^2/12$  is referred to as the uniform upper bound (UUB).

## 5.2. Experimental results

The structure of the proposed MAP estimator is dependent on the Gaussian approximation (14). In the limit of high SNR, Proposition 1 implies that (14) is asymptotically exact, regardless of the particular pdf of the noise samples added to the Gaussian signal samples when forming  $x[k]$  in (1). To validate this claim, Fig. 3 shows histograms of  $x[k]$  for different SNR values. These plots were obtained by adding uniformly distributed noise to a bandlimited audio signal generated using the model (47), with parameter values as in Table 1. Despite the non-Gaussian nature of the quantization noise, the

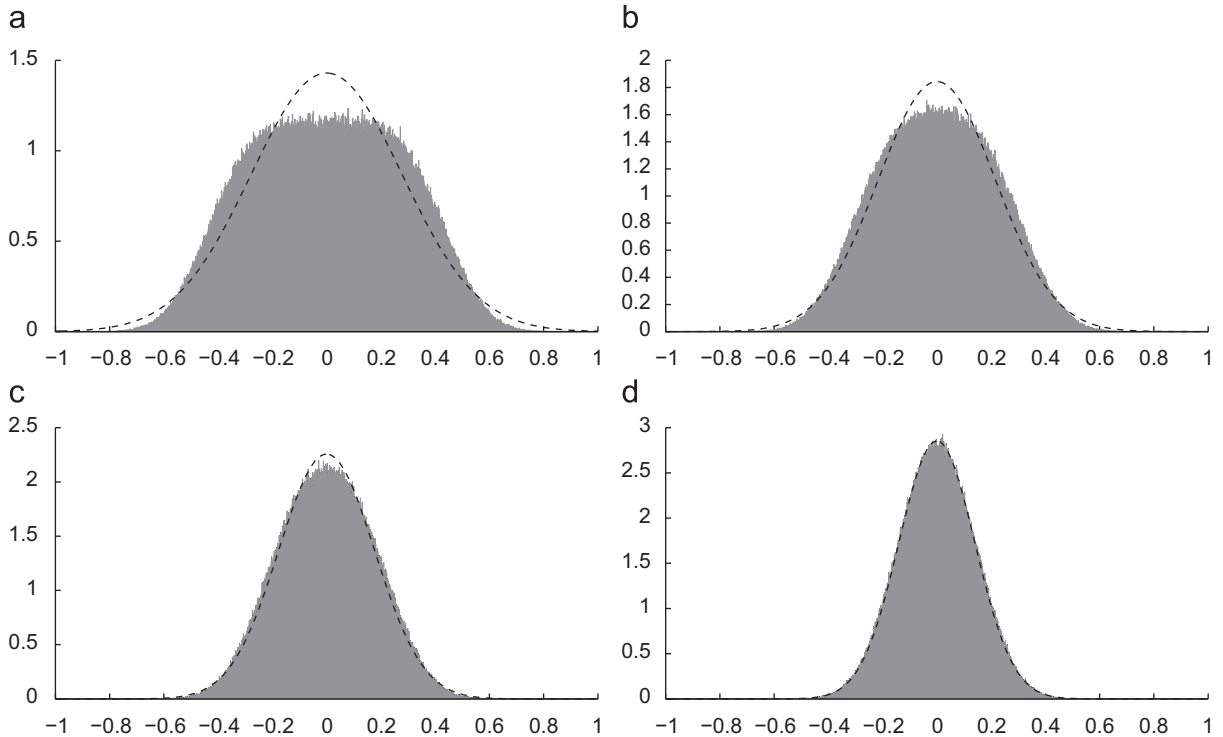


**Fig. 3.** Histograms of random bandlimited audio signal corrupted by additive uniform noise with different SNRs. The dashed line shows a Gaussian PDF with a variance matching the combined signal and noise variance. (a) SNR = -6 dB. (b) SNR = -3 dB. (c) SNR = 0 dB. (d) SNR = 6 dB.

noisy samples tend to a Gaussian distribution as the SNR increases, providing strong experimental support for Proposition 1.

Focusing now on the various crossing-point estimators, Fig. 4 shows their standard deviation (in units of the sampling period) as the interpolation window length  $M$  is varied. Except for ILIN, which uses a fixed value of  $M=2$ , all the other estimators use the same values of  $M, M_1$ , and  $M_2$ . As expected, their performance generally improves with  $M$ , up to a point where incorporating new data does not add new information due to loss of temporal correlation in the signal (about  $M=8$  here). The proposed MAP and MMSE estimators yield an almost identical performance, which approaches the fundamental limit predicted by the Bayesian CRB. A similar behavior is noted with the POL estimator but the performance is not as good, while the performance of both the SPL and ILIN saturates at a much higher level, consistent with the fact that they are based on linear and cubic interpolation, respectively. Fig. 5 shows the bias of these estimators under similar conditions. Comparing with Fig. 4, we note that the bias is always considerably smaller than the corresponding standard deviation. For practical purposes, these estimators may therefore be considered unbiased. In the sequel, we focus on MSE and do not present bias plots.

Fig. 6 shows the estimator performance as a function of the sampling frequency. The horizontal axis is normalized to the Nyquist rate, so that a value of 1 corresponds to critical sampling (i.e.  $f_s = 2f_m$ ). As above, the best performance is obtained with the proposed MAP and MMSE estimators. The POL and SPL estimators are superimposed on this plot since

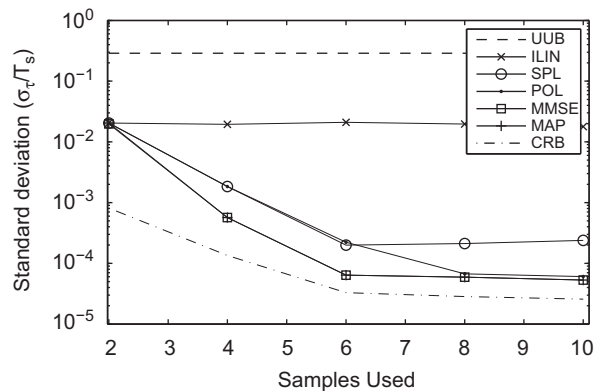


**Fig. 4.** Estimator variance: length  $M$  of vector  $\mathbf{x}$  varies.

$M=4$  samples are used. In the context of digitally controlled switching amplifiers, audio quality depends on the accuracy of crossing-point estimation. For example, in [16], the use of a 4-point polynomial crossing-point estimator is required to maintain a bound on distortion of -102 dB. However, this presumes a highly over-sampled input (i.e. 20 kHz bandwidth, sampled at 352.8 kHz). The MMSE estimator we propose outperforms POL by a wide enough margin. Consequently, a lower over-sampling rate may be adopted instead which will significantly reduce the overall system costs.

Fig. 7 shows the estimator performance as the SNR is varied. Again, the best results are obtained with the proposed MAP and MMSE estimators. In all cases, estimator performance improves as the SNR increases until it

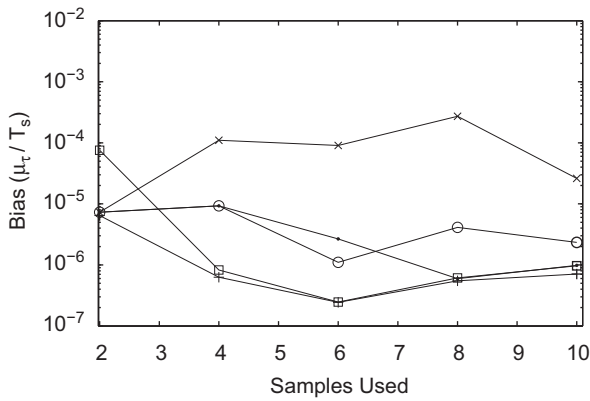


Fig. 5. Estimator bias: length  $M$  of vector  $\mathbf{x}$  varies.

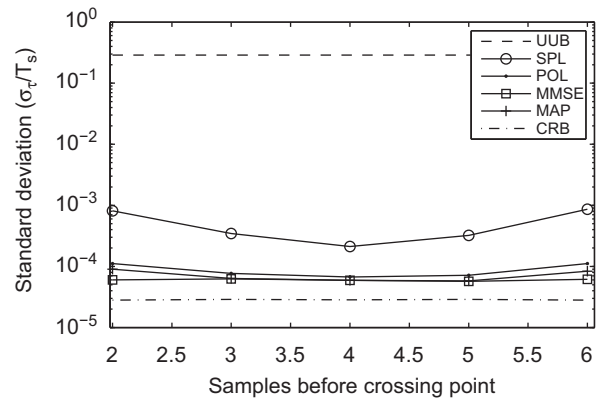


Fig. 8. Estimator performance: sample offset  $M_1$  varies.

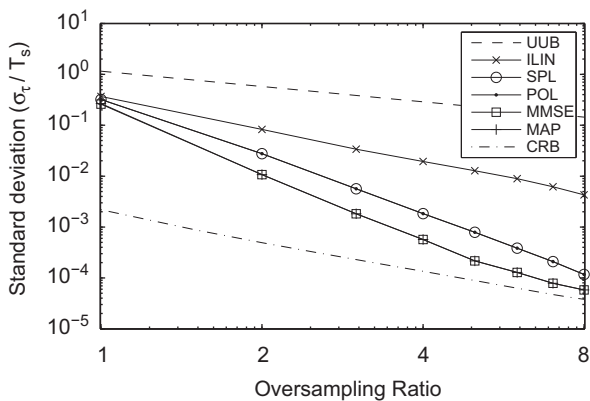


Fig. 6. Estimator performance: oversampling ratio varies.

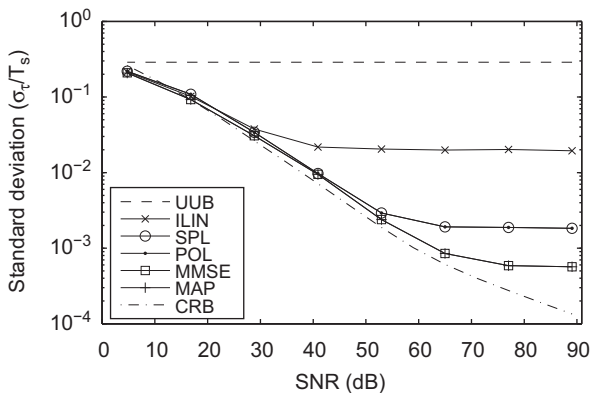


Fig. 7. Estimator performance: SNR varies.

saturates at a fixed level above the CRB. For both the POL, MMSE and MAP, the saturation level can be reduced by increasing  $M$  from 4 to 6. However, for a given  $M$ , the MAP and MMSE estimator always reach a significantly lower MSE level, i.e. by 6 dB or more. The results in Fig. 7 also indicate that the Bayesian CRB (35) provides a tight bound on system performance over a wide range of SNR values.

The ability of the MAP estimator to give accuracy close to the Bayesian CRB does not come as a surprise: indeed, the MAP uses a search procedure to optimize the same score function, the conditional pdf of the crossing point given the observed data, on which the derivation of the CRB is based [38].

Fig. 8 shows the estimator performance as a function of the offset parameter  $M_1$ . To better emphasize the effect of  $M_1$ , the number of samples  $M=M_1+M_2$  has been increased to 8 in this figure. The performance of the various estimators is seen to be optimal when the crossing point falls in the center of the observation vector, i.e.  $M_1=M_2=4$ . The MMSE estimator is the most robust to deviations from this optimum operating point.

## 6. Conclusion

We considered estimating the crossing points of a known function with a continuous-time random process, given uniformly spaced, noisy samples of this process. We derived the MAP estimator, along with an intuitively satisfying estimator based on MMSE considerations. The MMSE estimator was shown to be a lower-complexity approximation to the MAP estimator. We also derived the fundamental Bayesian CRB on the lowest attainable MSE for any estimator for the problem. Simulations of a PWM scenario demonstrated that MAP and MMSE outperformed commonly used polynomial estimators. The MAP and MMSE estimators were nearly unbiased and their MSE approached the Bayesian CRB, which provides a tight bound under practical conditions of operation. The MMSE is therefore a particularly attractive solution as it offers a nearly optimal, yet computationally efficient approximation to the MAP estimator.

The computational cost of implementing the proposed MAP and MMSE estimators is greatly dependent on the types of resource that silicon can provide. There are only a few broad classes of implementation device (e.g. FPGAs and DSPs) available to designers, and it would be worthwhile to investigate the balance between accuracy and computational efficiency for each device.

## Appendix A. Proof of Proposition 1

It is convenient to define the normalized random vector  $\mathbf{s}' \triangleq \sigma_s^{-1} \mathbf{s}$ ,  $\mathbf{n}' \triangleq \sigma_n^{-1} \mathbf{n}$  and  $\mathbf{x}' \triangleq \sigma_x^{-1} \mathbf{x}$  where  $\sigma_x^2 \triangleq \sigma_s^2 + \sigma_n^2$ . From (8), it follows that

$$\mathbf{x}' = \frac{\sigma_s}{\sigma_x} \mathbf{s}' + \frac{\sigma_n}{\sigma_x} \mathbf{n}'. \quad (\text{A.1})$$

Below, we derive an asymptotic expansion for the pdf of  $\mathbf{x}'$  in terms of the ratio  $\sigma_n/\sigma_x$ . We first recall the definition of the cumulant-generating function (cgf) of an  $M$ -dimensional random vector  $\mathbf{x}$  [52]:

$$K_{\mathbf{x}}(\boldsymbol{\omega}) = \ln E\{e^{j\boldsymbol{\omega}^T \mathbf{x}}\}, \quad (\text{A.2})$$

where  $\boldsymbol{\omega} = (\omega_1, \dots, \omega_M)^T$  is an  $M$ -dimensional vector of angular frequencies. Let  $K_{\mathbf{x}'}(\boldsymbol{\omega})$ ,  $K_{\mathbf{s}'}(\boldsymbol{\omega})$  and  $K_{\mathbf{n}'}(\boldsymbol{\omega})$  denote the cgf of  $\mathbf{x}'$ ,  $\mathbf{s}'$  and  $\mathbf{n}'$ , respectively. Under the current modeling assumptions for the signal and noise, we have

$$K_{\mathbf{x}'}(\boldsymbol{\omega}) = K_{\mathbf{s}'}\left(\frac{\sigma_s}{\sigma_x} \boldsymbol{\omega}\right) + K_{\mathbf{n}'}\left(\frac{\sigma_n}{\sigma_x} \boldsymbol{\omega}\right), \quad (\text{A.3})$$

$$K_{\mathbf{s}'}(\boldsymbol{\omega}) = -\frac{1}{2\sigma_s^2} \boldsymbol{\omega}^T \Sigma_s \boldsymbol{\omega}, \quad (\text{A.4})$$

$$K_{\mathbf{n}'}(\boldsymbol{\omega}) = -\frac{1}{2\sigma_n^2} \boldsymbol{\omega}^T \Sigma_n \boldsymbol{\omega} + R(\boldsymbol{\omega}), \quad (\text{A.5})$$

where the residual term  $R(\boldsymbol{\omega})$  admits a Taylor series expansion

$$R(\boldsymbol{\omega}) = \sum_{\nu=3}^{\infty} \left( \sum_{\substack{k_1 \dots k_M \\ \sum k_i = \nu}} \frac{\kappa_{k_1 \dots k_M}^{(\nu)}}{k_1! \dots k_M!} (j\omega_1)^{k_1} \dots (j\omega_M)^{k_M} \right). \quad (\text{A.6})$$

In (A.6), the inner summation is over all integers  $k_i \geq 0$  with  $\sum_{i=1}^M k_i = \nu$  and the coefficients  $\kappa_{k_1 \dots k_M}^{(\nu)}$  are the cumulants of order  $\nu$  of  $\mathbf{n}'$ . Substituting (A.4)–(A.6) into (A.3), we obtain

$$K_{\mathbf{x}'}(\boldsymbol{\omega}) = -\frac{1}{2\sigma_x^2} \boldsymbol{\omega}^T \Sigma_x \boldsymbol{\omega} + R\left(\frac{\sigma_n}{\sigma_x} \boldsymbol{\omega}\right). \quad (\text{A.7})$$

Taking the exponential of (A.7) gives the characteristic function of  $\mathbf{x}'$ :

$$\begin{aligned} \psi_{\mathbf{x}'}(\boldsymbol{\omega}) &= e^{-(1/2\sigma_x^2)\boldsymbol{\omega}^T \Sigma_x \boldsymbol{\omega}} e^{R(\sigma_n/\sigma_x \boldsymbol{\omega})} \\ &= e^{-(1/2\sigma_x^2)\boldsymbol{\omega}^T \Sigma_x \boldsymbol{\omega}} \left( 1 + R\left(\frac{\sigma_n}{\sigma_x} \boldsymbol{\omega}\right) + \frac{1}{2!} \left[ R\left(\frac{\sigma_n}{\sigma_x} \boldsymbol{\omega}\right) \right]^2 + \dots \right) \\ &= e^{-(1/2\sigma_x^2)\boldsymbol{\omega}^T \Sigma_x \boldsymbol{\omega}} \left( 1 + \frac{\sigma_n^3}{\sigma_x^3} \sum_{\substack{k_1 \dots k_M \\ \sum k_i = 3}} \frac{\kappa_{k_1 \dots k_M}^{(3)}}{k_1! \dots k_M!} (j\omega_1)^{k_1} \dots (j\omega_M)^{k_M} + \dots \right). \end{aligned} \quad (\text{A.8})$$

The above series is apperanted to the so-called Edgeworth's expansion used in the derivation of an asymptotic expression for the pdf of a sum of a large number of independent random variables [30]. The desired expansion for the pdf of  $\mathbf{x}'$  is obtained by inverse Fourier transformation of (A.8), i.e.:

$$f_{\mathbf{x}'}(\boldsymbol{\xi}) = \phi(\boldsymbol{\xi}; \sigma_x^{-2} \Sigma_x) - \frac{\sigma_n^3}{\sigma_x^3} \sum_{\substack{k_1 \dots k_M \\ \sum k_i = 3}} \frac{\kappa_{k_1 \dots k_M}^{(3)}}{k_1! \dots k_M!} \frac{\partial^3 \phi(\boldsymbol{\xi}; \sigma_x^{-2} \Sigma_x)}{\partial \xi_1^{k_1} \dots \partial \xi_M^{k_M}} + \dots, \quad (\text{A.9})$$

where, for an arbitrary positive definite  $M \times M$  covariance matrix  $\Sigma$ , we define the multi-variate Gaussian distribution

$$\phi(\boldsymbol{\xi}; \Sigma) = \frac{1}{(2\pi)^{M/2} |\Sigma|^{1/2}} e^{-(1/2)\boldsymbol{\xi}^T \Sigma^{-1} \boldsymbol{\xi}}. \quad (\text{A.10})$$

The pdf of the original observation vector  $\mathbf{x}$  is finally obtained as

$$f_{\mathbf{x}}(\boldsymbol{\xi}) = \frac{1}{\sigma_x^M} f_{\mathbf{x}'}\left(\frac{1}{\sigma_x} \boldsymbol{\xi}\right). \quad (\text{A.11})$$

This completes the proof.

## References

- [1] L.R. Rabiner, R.W. Shafer, Digital Processing of Speech Signals, Prentice Hall, 1978.
- [2] T.V. Sreenivas, R.J. Niederjohn, Zero-crossing based spectral analysis and SVD spectral analysis for formant frequency estimation in noise, IEEE Transactions on Signal Processing 40 (1992) 282–293.
- [3] B. Kedem, Spectral analysis and discrimination by zero-crossings, Proceedings of the IEEE 74 (1986) 1477–1493.
- [4] G.E. Mog, E.P. Ribeiro, Zero crossing determination by linear interpolation of sampled sinusoidal signals, in: Proceedings of the IEEE/PES Transmission and Distribution Conference and Expo: Latin America, Nov. 2004, pp. 799–802.
- [5] S.C. Sekhar, T.V. Sreenivas, Auditory motivated level-crossing approach to instantaneous frequency estimation, IEEE Transactions on Signal Processing 53 (2005) 1450–1461.
- [6] R.G. Wiley, H. Schwarzlander, D.D. Weiner, Demodulation procedure for very wide-band FM, IEEE Transactions on Communications 25 (1977) 318–327.
- [7] H.M. Kwon, E.K.B. Lee, A novel digital FM receiver for mobile and personal communications, IEEE Transactions on Communications 44 (1996) 1466–1476.
- [8] T. Scholand, A. Burnic, C. Spiegel, A. Waadt, A. Hessamian-Alinejad, P. Jung, Applying zero-crossing demodulation to the bluetooth enhanced data rate mode, in: Proceedings of the 17th IEEE International Symposium on Personal, Indoor and Mobile Radio Communications, Sept. 2006, 5 pp.
- [9] I. Blake, W. Lindsey, Level-crossing problems for random processes, IEEE Transactions on Information Theory 19 (1973) 295–315.
- [10] N. Sayiner, H.V. Sorensen, T.R. Viswanathan, A level-crossing sampling scheme for A/D conversion, IEEE Transactions on Circuits and Systems—II 43 (1996) 335–339.
- [11] K.M. Guan, A.C. Singer, Opportunistic sampling by level-crossing, in: Proceedings of the IEEE International Conference on Acoustics, Speech and Signal Processing, vol. 3, pp. 1513–1516.
- [12] I. Bar-David, An implicit sampling theorem for bounded bandlimited functions, Information and Control 24 (1974) 36–44.
- [13] A.J. Rainal, Origin of Rice's formula, IEEE Transactions on Information Theory 34 (1988) 1383–1387.
- [14] B.F. Logan, Click modulation, AT&T Bell Laboratories Technical Journal 63 (1984) 401–423.
- [15] J.M. Goldberg, M.B. Sandler, New high accuracy pulse width modulation based digital-to-analogue converter/power amplifier, IEE Proceedings—Circuits, Devices & Systems 141 (1994) 315–324.
- [16] C. Pascual, Z. Song, P.T. Krein, D.V. Sarwate, P. Midya, W. Roekner, High-fidelity PWM inverter for digital audio amplification based on real-time DSP: Spectral analysis, real-time DSP implementation, and results, IEEE Transactions on Power Electronics 18 (2003) 473–485.
- [17] F. Marvasti, M. Sandler, Applications of nonuniform sampling to nonlinear modulation A/D and D/A techniques, in: F. Marvasti (Ed.), Nonuniform Sampling, Kluwer Academic, 2001, pp. 647–697.
- [18] A.M. Stankovic, G.C. Verghese, R.O. Hinds, Monte-Carlo verification of power spectrum formulas for random modulation schemes, in: Proceedings of the IEEE Workshop on Computers in Power Electronics, Aug. 1992, pp. 187–194.
- [19] Z. Song, D.V. Sarwate, The frequency spectrum of pulse width modulated signals, Signal Processing 83 (2003) 2227–2258.
- [20] G.C. Verghese, V.J. Thottuvelil, Aliasing effects in PWM power converters, in: Proceedings of the IEEE Power Electronics Specialists Conference, vol. 2, 1999, pp. 1043–1049.
- [21] S. Santi, R. Rovatti, G. Setti, Spectral aliasing effects of PWM signals with time-quantized switching instants, in: Proceedings of the

- International Symposium on Circuits and Systems, vol. 4, May 2004, pp. 689–692.
- [22] A. Floros, J. Mourjopoulos, Distortion-free 1-bit PWM coding for digital audio signals, *EURASIP Journal on Advances in Signal Processing* 2007 (2007) 1–12.
- [23] B.-H. Gwee, J.S. Chang, V. Adrian, A micropower low-distortion digital class-D amplifier based on an algorithmic pulsewidth modulator, *IEEE Transactions on Circuits and Systems—I* 52 (2005) 2007–2022.
- [24] C. Pascual, B. Roeckner, Computationally efficient conversion from pulse-code-modulation to naturally-sampled pulse-width-modulation, in: *Proceedings of the 109th Convention of the Audio Engineering Society*, Sept. 2000.
- [25] V. Shimanskiy, S.-C. Jang, Iterative method for natural sampling, in: *Proceedings of the 121st Convention of the Audio Engineering Society*, Oct. 2006, 6 pp.
- [26] P. Midya, B. Roeckner, P. Rakers, P. Wagh, Prediction correction algorithm for natural pulse width modulation, in: *Proceedings of the 109th Convention of the Audio Engineering Society*, Sept. 2000.
- [27] E. Bresch, W.T. Padgett, TMS320C67-based design of a digital audio power amplifier introducing a novel feedback strategy, Technical Report, Rose-Hulman Institute of Technology, Indiana, 2002, 16 pp.
- [28] K.C. Nguyen, D.V. Sarwate, Up-sampling and natural sample value computation for digital pulse width modulators, in: *Proceedings 40th Annual Conference on Information Sciences and Systems*, Mar. 2006, pp. 1096–1101.
- [29] S.V. Vaseghi, *Advanced Signal Processing and Noise Reduction*, Wiley, 2008.
- [30] C. Field, E. Ronchetti, *Small Samples Asymptotics*, Institute of Mathematical Statistics, CA, 1990.
- [31] J.G. Proakis, D.G. Manolakis, *Digital Signal Processing: Principles, Algorithms and Applications*, fourth ed., Prentice Hall, 2007.
- [32] A. Gelb, W.E.V. Velde, *Multiple-Input Describing Functions and Nonlinear System Design*, McGraw-Hill, 1968.
- [33] D. Hatzinakos, Blind deconvolution: channel identification and equalization, in: C.T. Leondes (Ed.), *Digital Signal Processing Systems: Implementation Techniques*, Academic Press, 1995.
- [34] S.H. Ardalan, J.J. Paulos, An analysis of nonlinear behavior in delta-sigma modulators, *IEEE Transactions on Circuits and Systems* 34 (1987) 593–603.
- [35] R. Khoini-Poorfard, D.A. Johns, Analysis of  $\sigma\delta$  modulators with zero mean stochastic inputs, *IEEE Transactions on Circuits and Systems—II* 42 (1995) 164–175.
- [36] J. Markus, P. Deval, V. Quiquempoix, J. Silva, G.C. Temes, Incremental delta-sigma structures for DC measurement: an overview, in: *Proceedings IEEE Custom Integrated Circuits Conference*, Sept. 2006, pp. 41–48.
- [37] A. Papoulis, S.U. Pillai, *Probability, Random Variables and Stochastic Processes*, McGraw-Hill, 2002.
- [38] H.L. Van Trees, *Detection, Estimation, and Modulation Theory—Part I*, John Wiley and Sons, Inc., 1968.
- [39] Y.L. Tong, *The Multivariate Normal Distribution*, Springer, 1990.
- [40] G. Golub, C. Van Loan, *Matrix Computations*, Johns Hopkins University Press, 1996.
- [41] W.H. Press, *Numerical Recipes in C*, Cambridge University Press, 1988.
- [42] S. Haykin, *Adaptive Filter Theory*, Prentice Hall, 1991.
- [43] R.D. Gill, B.Y. Levit, Applications of the van Trees inequality: a Bayesian Cramér–Rao bound, *Bernoulli* 1 (1995) 59–79.
- [44] E.J. Dudewicz, S.N. Mishra, *Modern Mathematical Statistics*, Wiley, 1998.
- [45] S. Kay, *Fundamentals of Statistical Signal Processing*, vol. 1, Prentice-Hall, 1993.
- [46] D. Slepian, H.O. Pollak, Prolate spheroidal wave functions, Fourier analysis and uncertainty—I, *Bell System Technical Journal* 40 (1961) 43–63.
- [47] G. Smecher, Discrete-time crossing-point estimation for switching power converters, Master's Thesis, McGill University, 2008.
- [48] R.W. Schafer, L.R. Rabiner, A digital signal processing approach to interpolation, *Proceedings of the IEEE* 61 (1973) 692–702.
- [49] T.I. Laakso, V. Valimaki, M. Karjalainen, U.K. Laine, Splitting the unit delay, *IEEE Signal Processing Magazine* 13 (1996) 30–60.
- [50] E. Meijering, A chronology of interpolation: from ancient astronomy to modern signal and image processing, *Proceedings of the IEEE* 90 (2002) 319–342.
- [51] C. de Boor, *A Practical Guide to Splines*, Springer, 1978.
- [52] J.M. Mendel, Tutorial on higher-order statistics (spectra) in signal processing and system theory: theoretical results and some applications, *Proceedings of the IEEE* 79 (1991) 278–305.